Quantum Mechanical/Molecular Mechanical Study on the Mechanisms of Compound I Formation in the Catalytic Cycle of Chloroperoxidase: An Overview on Heme Enzymes

Hui Chen,[†] Hajime Hirao,[†] Etienne Derat,[†,§] Ilme Schlichting,[‡] and Sason Shaik*,[†]

Institute of Chemistry and The Lise Meitner-Minerva Center for Computational Quantum Chemistry, The Hebrew University of Jerusalem, Givat Ram Campus, 91904 Jerusalem, Israel, and Department of Biomolecular Mechanisms, Max Planck Institute for Medical Research, Jahnstrasse 29, 69120 Heidelberg, Germany

Received: April 7, 2008; Revised Manuscript Received: May 11, 2008

The formation of Compound I (Cpd I), the active species of the enzyme chloroperoxidase (CPO), was studied using QM/MM calculation. Starting from the substrate complex with hydrogen peroxide, Fe^{III}−HOOH, we examined two alternative mechanisms on the three lowest spin-state surfaces. The calculations showed that the preferred pathway involves heterolytic O−O cleavage that proceeds via the iron hydroperoxide species, i.e., Compound 0 (Cpd 0), on the doublet-state surface. This process is effectively concerted, with a barrier of 12.4 kcal/mol, and is catalyzed by protonation of the distal OH group of Cpd 0. By comparison, the path that involves a direct O−O cleavage from Fe^{III}−HOOH is less favored. A proton coupled electron transfer (PCET) feature was found to play an important role in the mechanism nascent from Cpd 0. Initially, the O−O cleavage progresses in a homolytic sense, but as soon as the proton is transferred to the distal OH, it triggers an electron transfer from the heme-oxo moiety to form water and Cpd I. This study enables us to generalize the mechanisms of O−O activation, elucidated so far by QM/MM calculations, for other heme enzymes, e.g., cytochrome P450cam, horseradish peroxidase (HRP), nitric oxide synthase (NOS), and heme oxygenase (HO). Much like for CPO, in the cases of P450 and HRP, the PCET lowers the barrier below the purely homolytic cleavage alternative (in our case, the homolytic mechanism is calculated directly from Fe^{III}−HOOH). By contrast, the absence of PCET in HO, along with the robust water cluster, prefers a homolytic cleavage mechanism.

1. Introduction

Chloroperoxidase (CPO)[1–3] is a heme peroxidase from the marine fungus *Caldariomyces fumago.* It is unique in catalyzing the hydrogen peroxide-dependent halogenation reaction (Cl^-, Br^-, and I^-) of organic substrates such as β-diketones,[4] alkenes,[5] alkynes,[6] anilines, phenols, and heterocyclics.[7] Recent studies revealed that CPO also catalyzes dehalogenation reactions.[8] Unlike other peroxidases, CPO has a cysteine-derived thiolate ligand as the proximal ligand for its prosthetic heme group,[9] similar to the related monooxygenases cytochrome P450[2,10] and the nitric oxide synthase (NOS).[11] In fact, CPO is capable of catalyzing many P450 reactions: these include heteroatom dealkylation,[12] benzylic,[13] and propargylic[14] hydroxylation, alkene epoxidation,[15] sulfoxidation,[16] and N-oxidation of arylamines.[17] One advantage of CPO over P450 as a potential green monooxygenase is that CPO uses H_2O_2 as the oxygen source and hence does not require the activation of O_2 by reducing cofactors, e.g., NADPH and diiron−disulfur clusters and proton sources, which are needed by P450s. Being a peroxidase with a polar distal pocket, CPO can also undergo classical peroxidase reactions with one-electron oxidizable substrates such as ascorbate and phenols[18] and catalase reactions of two-electron oxidation such as the H_2O_2 dismutation.[19]

SCHEME 1: Cpd I of CPO

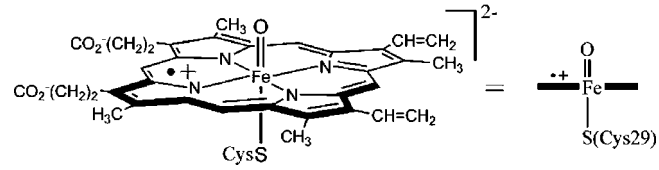

It is widely accepted that reactions catalyzed by CPO are mediated by the active reaction intermediate, termed Compound I (Cpd I), shown in Scheme 1, which possesses two oxidation equivalents above the ferric resting state.[20] Although Cpd I of CPO is short-lived, it is the only Cpd I of thiolate-ligated enzymes that is well characterized by many spectroscopic methods including UV/vis absorption,[21,22a] EPR, Mössbauer,[23] and resonance Raman.[22] Since CPO and P450 share the same proximal thiolate ligand for heme, they also have many spectroscopic similarities.[24] Therefore, the information from Cpd I of CPO may be relevant to the putative and elusive P450 Cpd I species.[2,10,25]

CPO combines the peroxidase-type active site heme environment with a P450 type axial ligand.[26] In contrast to other peroxidases, CPO not only contains an untypical proximal ligand but also lacks the two conserved distal residues of a histidine and an arginine, found normally in peroxidases. These residues are considered to play important roles in O−O cleavage to generate Cpd I in the Poulos−Kraut mechanism of peroxidase activity.[27] Instead, a glutamate residue (Glu183, see Figure 1) was found in the distal pocket of CPO at a position not far

* Corresponding author. E-mail: sason@yfaat.ch.huji.ac.il.
[†] The Hebrew University of Jerusalem.
[‡] Max Planck Institute for Medical Research.
[§] Current address: Laboratoire de Chimie Organique, Institut de Chimie Moléculaire, Université Pierre et Marie Curie-Paris 6, 4 place Jussieu B. 229, 75005 Paris, France.

10.1021/jp803010f CCC: $40.75
Published on Web 07/03/2008

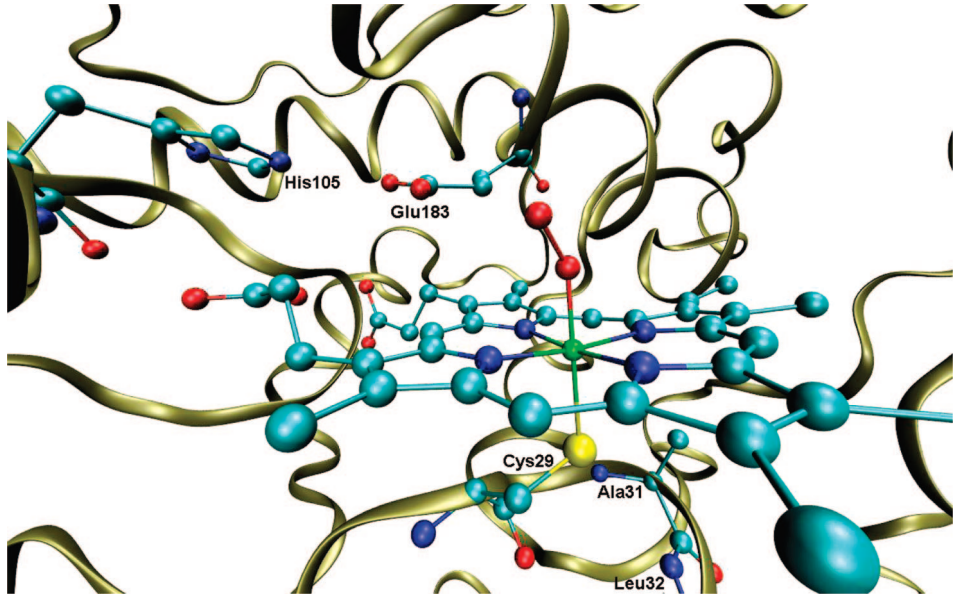

Figure 1. Active site of CPO showing the $Fe^{III}OO$ moiety of $Fe^{III}OOH$ (PDB code 2J5M).

away from the Fe atom (about 5 Å). A histidine (His105) residue is located near Glu183, but is too far away from the Fe center to directly be involved in the O−O activation processes starting from the Fe coordinated H_2O_2. The function of His105 was postulated to involve the fixing of Glu183 and modulating the acidity of this residue.[28]

Like other peroxidases, in CPO the precursor of Cpd I is iron-coordinated H_2O_2. Experiments with the Glu183His mutant show that Glu183 has a function similar to that of the distal histidine residue in the other peroxidases.[29] It was proposed by Sundaramoorthy et al. that Glu183 plays a double role of both proton donor and acceptor to Fe-HOOH (the Fe-coordinated H_2O_2) when generating the catalytically active species Cpd I.[30] Thus, Glu183 is thought to act as a shuttle that delivers the proton of the proximal O atom of the Fe-HOOH complex to the distal O atom to facilitate heterolytic cleavage of the O−O bond. This proposal is similar to the Poulos−Kraut mechanism for Cpd I formation in peroxidases.[27] In the current work, we analyze this proposal by the QM/MM method.

In an early theoretical treatment of the CPO reaction mechanism, Filizola and Loew[31] used classical molecular dynamic (MD) simulations to explore the role of the protein in Cpd I formation. Indeed, in accord with the preceding proposal,[30] the distal residue Glu183 was found to possibly have a dual role; first as proton acceptor and then as proton donor. However, the detailed reaction process of Cpd I formation was not explored because of the inherent limitations of the classical MD method based on molecular mechanics (MM) to study chemical reaction processes. The chemical bond breaking and formation processes as encountered here for Cpd I formation require a quantum mechanics (QM)-based method. As such, we present here a detailed theoretical study on the formation of Cpd I in CPO using a hybrid quantum mechanical/molecular mechanical (QM/MM) approach. The QM/MM methodology combines the ability of the QM method to describe the chemical reaction with the efficiency of the MM method in treating the protein environment of the enzyme and hence should be an appropriate tool for investigating the mechanisms of enzymatic reactions.[32] Thus, the present work addresses the following unresolved issues: (a) the question of homolytic versus heterolytic O−O cleavage in Cpd I formation.[25a,33] (b) Is there any other pathway that leads to Cpd I other than the generally accepted ferric hydroperoxide intermediate, Fe^{III}−OOH, the so-called Compound 0 (Cpd 0) species? (c) What is the function of His105 in Cpd I formation? (d) What is the transition state (TS) in the most preferred pathway to Cpd I? These questions are addressed in the present study by performing detailed mechanistic explorations on the low-lying three spin states. In turn, the so-derived QM/MM mechanism of Cpd I formation in CPO will be compared to previous QM/MM-determined mechanisms for other heme enzymes such as P450,[34] NOS,[35] horseradish peroxidase (HRP),[36] heme oxygenase (HO),[37] and catalase (CAT)[38] with an aim of providing an overview for heme enzymes.

2. Computational Details

2.1. QM/MM Methodology and Software. The QM/MM calculations were done using ChemShell[39] interfaced to Turbomole[40] and DL_POLY,[41] which together handle the QM and MM calculations. The hybrid B3LYP[42] functional was used throughout this study for the QM part, and the CHARMM22 force field[43] was used for the MM part. The active region of the enzyme that is described by a QM method further interacts with the rest of the enzyme (MM part) by electrostatic and van der Waals/Lennard−Jones interactions. The electronic embedding scheme was used to account for the polarization effect of the QM part induced by the protein environment. The dangling bond at the QM/MM boundary was saturated by a hydrogen-link atom and treated in the framework of the charge-shift method.[44]

QM/MM geometry optimization was performed using a double-ζ basis set (LACVP)[45] for all atoms except the two oxygen atoms coordinated to the iron and the oxygen atom in Glu183 hydrogen-bonded to the Fe^{III}−HOOH center, for which we used a double-ζ basis set augmented with polarization and diffuse functions (6−31+G(d)).[46] The latter augmentation is, in our experience, essential for a better description of the important O−O cleavage process. This basis set is henceforth called B1. The energy was corrected by QM/MM single point calculations with a larger basis set B2, which describes iron by the Wachters all electron basis set,[47] augmented with diffuse d and polarization f functions, and the rest of the atoms by the 6-31++G(d,p) basis set.

2.2. Setup of the System. To prepare suitable initial structures for the QM/MM calculations, we started from the experimentally determined crystal structure of the Cpd 0 complex of CPO (PDB code 2J5M).[48] We built a complete model of solvated enzyme by adding missing hydrogen atoms and a 16-Å-thick water solvent layer. The system was further prepared according to standard procedures (see the Supporting Information document). The entire system consisted of 18,338 atoms, including 12,735 atoms in the solvent part. This system was then relaxed by performing pure force field molecular dynamics (MD) and MM minimization calculations with the CHARMM22 force field as implemented in the CHARMM program,[49] during which the coordinates of the heme, the proximal ligand Cys29, and the outer 8-Å-thick water solvent layer were kept fixed. The MD calculations did not modify the structure significantly compared to the initial X-ray structure. Therefore, we performed the QM/MM calculations on the coordinates obtained after simple force field energy minimizations and short MD on the inner solvent layer (in order to remove close contacts) and not on the coordinates that were obtained after equilibration by long MD simulations.

2.3. Charged Residues and Total Charge of the System. The total charge of the so-generated system was −16, corresponding to the following protonation states of various residues: aspartic acid (Asp) and glutamic acid (Glu) residues were assumed to be ionized, i.e., negatively charged (Asp11, Asp24, Asp44, Asp86, Asp89, Asp106, Asp113, Asp123, Asp126, Asp131, Asp140, Asp149, Asp152, Asp168, Asp193, Asp198, Asp200, Asp208, Asp291, Asp298, Glu1, Glu51, Glu69, Glu80, Glu99, Glu104, Glu133, Glu155, Glu161, Glu166, Glu175, Glu183, Glu201, Glu217, Glu233, Glu235, and Glu266); and arginine (Arg) and lysine (Lys) residues were used as positively charged (Arg26, Arg46, Arg50, Arg111, Arg128, Arg157, Arg160, Arg206, Arg232, Lys112, Lys115, Lys145, Lys177, and Lys211). The histidine residues (His38, His43, His60, His101, His105, His107, His147, His222, and His226) were doubly protonated, and hence, each of them had one positive charge. There are two negative charges on the heme moiety, one negative charge on an acetate molecule near the pocket of the enzyme, and two positive charges on the Mn^{2+} ion coordinated to one of the propionate side chains of the protoporphyrin.

We tested the effect of the protonation state on the results by performing calculations on a neutral enzyme as well (using an alternative titratable residue protonation scheme described in the Supporting Information). The energetic results of the neutral enzyme were virtually the same (within 1.1 kcal/mol) as those for the −16 charged enzyme described above.

2.4. QM Region. Our chosen QM part comprises an iron−hydrogen peroxide porphyrin complex (without the side chains of heme) with its proximal ligand Cys29 (modeled as HS^-), the distal ligand His105 (modeled as protonated imidazole) and Glu183 (modeled as CH_3COO^-), which forms a hydrogen bond (H-bond) with the H_2O_2 coordinated to the iron. The QM region is illustrated in Scheme 2. The protonation state of His105 was determined, as such, from the fact that, in the X-ray structure, the $N_{imidazole}$—$O_{Glu/Asp}$ distances from the imidazole nitrogen atoms to one of the carboxylic oxygen atoms of Glu183 and one of Asp106 (main chain peptide bond, not shown in Scheme 2) were very short (2.62 Å and 2.75 Å), thus requiring H-bonding. The protonation state of His105 is also in line with the fact that the enzyme functions in acidic pH.

2.5. Optimized QM/MM Region. In addition to the QM region, seven additional residues and three crystal waters around the heme were allowed to relax in the QM/MM geometry optimization. As a result, the total QM/MM region included Ala27, Pro28, Cys29 (for technical reasons, this residue includes heme and H_2O_2), Pro30, Ala31, Leu32, Phe103, His105, Glu183, Phe186, W15, W22, and W37. The choice of these residues was made on the basis of the apparent interactions of these residues with the active species, in Scheme 2, by hydrogen bond, electrostatics, and Lennard−Jones interactions. The choice of the optimized MM part ensured that the relative QM-energies remained close to the relative total QM/MM energies (see Table S2 in the Supporting Information).

SCHEME 2: Schematic View of the QM Region (Totally Neutral) Used in the QM/MM Calculations

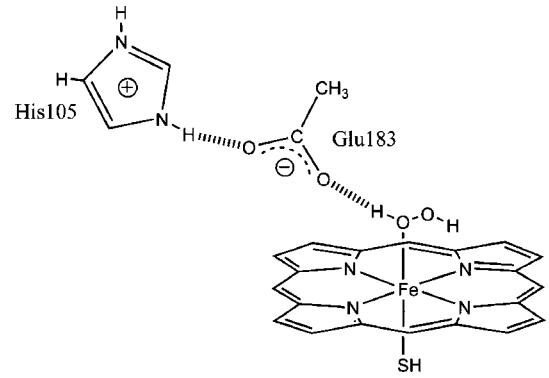

3. Results

To determine the mechanism of Cpd I formation in CPO, we examined two alternative pathways. The first one (Mechanism I) involves the formation of Cpd 0 and its conversion to Cpd I by heterolytic O−O bond cleavage. The second one (Mechanism II) generates Cpd I directly by a homolytic O−O bond cleavage within the Fe^{III}−HOOH moiety as found recently in some other systems.[35,50] These mechanisms were investigated for three spin states with $S = 1/2$, 3/2, and 5/2, namely, doublet, quartet and sextet, respectively. (In this work, the left-hand superscript of each species label signifies the spin multiplicity using the $2S+1$ value.) The first two states are the almost degenerate ground states for Cpd I, while the sextet state is quite stable for the Fe^{III}−HOOH complex and low lying for Cpd I.[51] The two mechanisms, the three spin states, and the two basis sets (B1 and B2) generate a great deal of data. To summarize these data in a fairly condensed form, we present in Figure 2 the energy profiles for the two mechanisms, three spin states, and two basis sets. Subsequently, we present in a stepwise manner a more detailed outline of the results for the various pathways, routinely using only the highest level B2//B1 data. More technical details are collected in the Supporting Information document deposited with this article.

3.1. Mechanism I: Cpd I Formation through Cpd 0. ***3.1.1. Iron Coordinated Hydrogen Peroxide Reactant Fe^{III}−HOOH.*** Since CPO employs hydrogen peroxide (H_2O_2) as an oxygen source, we started our mechanistic exploration from an iron-coordinated hydrogen peroxide species Fe^{III}−HOOH. In Figure 2, we show the calculated QM/MM relative energies of different spin states of this species. In addition, there can be two different types of conformations, shown in Scheme 3, whereby H_2O_2 coordinates to Fe in the heme, depending on which hydrogen moiety of H_2O_2 forms a hydrogen-bonding (H-bond) interaction with the carboxyl oxygen of the Glu183 residue. In the Fe^{III}−HOOH species labeled **1** (Type **1**), the H atom attached to the proximal O forms a H-bond with the

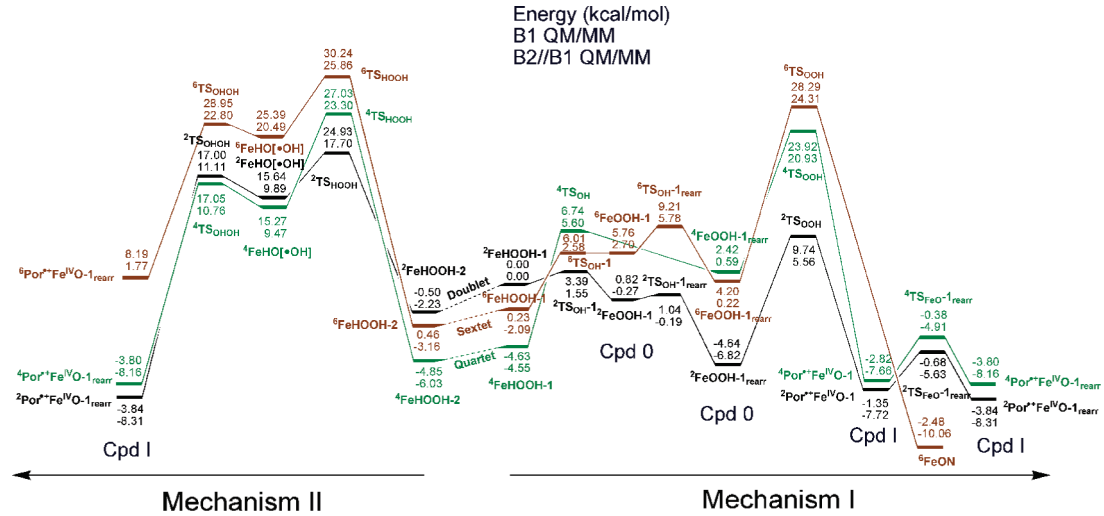

Figure 2. An overview of the UB3LYP/MM mechanisms for Cpd I formation in CPO. The relative energies of the species are given for the B1 and B2 basis sets, as specified on top of the figure.

SCHEME 3: Two Types of Conformations (Types 1 and 2) of Fe^{III}−HOOH and the Possible Subsequent Deprotonation Processes in CPO[a]

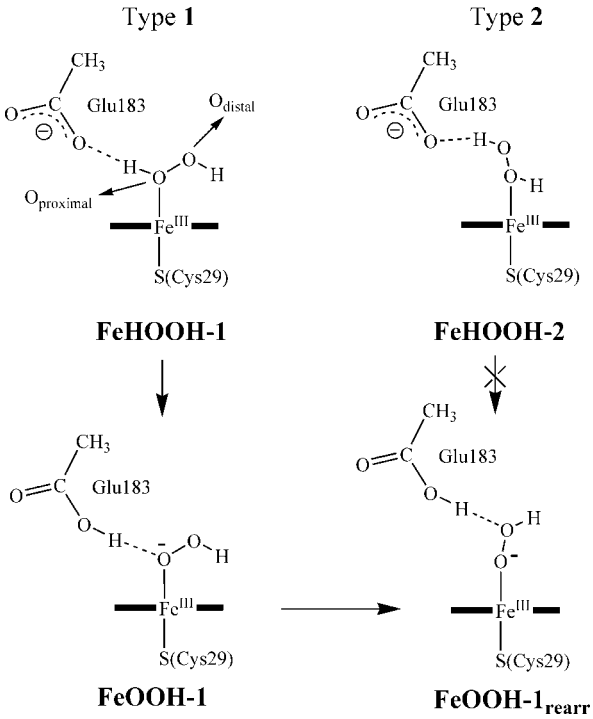

[a] The horizontal bold line represents the porphyrin ring.

carboxyl group of Glu183. In the second conformation designated as **2** (Type **2**), the H-bond with the carboxyl group of Glu183 involves the distal hydrogen. From Figure 2, one can see that, although the three states lie within a range of less than 5 kcal/mol, in both types of the Fe^{III}−HOOH species, the ground-state is the quartet state, the second lowest is the sextet state, and the doublet state is the highest of the three spin states. Table 1 summarizes the key bond distances in the optimized QM/MM geometries of Fe^{III}−HOOH. One can see that for the quartet and sextet states, the Fe−O and Fe−S bond distances are longer than those in the doublet state, which is consistent with the Fe−O and Fe−S antibonding character of the singly occupied $\sigma^*_{z^2}$ orbital in those two states. In the sextet state, the average Fe−N_{por} bond distance is about 0.05 Å longer than those

TABLE 1: Key Bond Distances *R* (in Å) of the Three Spin States of the Fe^{III}−HOOH Species[a]

		R (Fe−S)	*R* (Fe−O)	*R* (O−O)	R_{av} (Fe−N_{por})[b]	*R* (O−H)[c]
Type **1**	^{2}**FeHOOH-1**	2.391	2.163	1.455	2.025	1.687
	^{4}**FeHOOH-1**	2.545	2.469	1.453	2.024	1.728
	^{6}**FeHOOH-1**	2.479	2.488	1.454	2.079	1.742
Type **2**	^{2}**FeHOOH-2**	2.359	2.101	1.455	2.027	1.668
	^{4}**FeHOOH-2**	2.534	2.563	1.452	2.022	1.694
	^{6}**FeHOOH-2**	2.462	2.590	1.452	2.076	1.699

[a] The left-hand superscript signifies the spin state of the species. [b] The average value of the four Fe−N_{por} bond distances. [c] The H-bond between the carboxyl of Glu183 and H_2O_2 moiety.

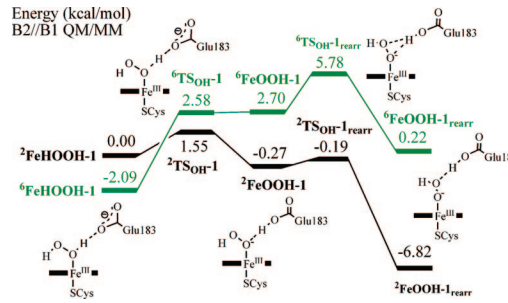

Figure 3. Energy profiles for the formation and conformational rearrangement of Cpd 0 (FeOOH) from FeHOOH. The relative energies are given for each species for the B2 basis set.

in the doublet and the quartet state, which is due to the Fe−N_{por} antibonding character of the singly occupied σ^*_{xy} in the sextet state.

3.1.2. Formation of Cpd 0 (Fe^{III}−OOH). Since only type **1** Fe^{III}−HOOH is H-bonded to Glu183 (Scheme 3) via the proximal OH, this conformation is the appropriate one to form Cpd 0 by deprotonation of the H-bonded hydrogen moiety. We therefore used this conformation to study the conversion of Fe^{III}−HOOH to Cpd 0. Initially, we performed a QM/MM energy scan along the O−H bond distance as the reaction coordinate (see Figure S1 in the Supporting Information). The results for the doublet and sextet states are shown in Figure 3 using B2 data (B1 data can be seen using the overall reaction scheme in Figure 2). The difference between the doublet and sextet states is apparent; in the doublet state, after an energy rise of 1.55 kcal/mol, Glu183 abstracts the proximal proton via

TABLE 2: Key Bond Distances *R* (in Å) of the Three Spin States of Cpd 0[a]

	R(Fe−S)	*R*(Fe−O)	*R*(O−O)	$R(O_{prox}-H)$[b]	$R(O_{dist}-H)$[c]	$R_{av}(Fe-N_{por})$[d]
^{2}FeOOH-1	2.500	1.897	1.463	1.697	2.109	2.032
^{6}FeOOH-1	2.597	2.101	1.452	1.520	2.159	2.089
^{2}FeOOH-1$_{rearr}$	2.490	1.850	1.463	2.515	1.646	2.031
^{4}FeOOH-1$_{rearr}$	2.700	2.066	1.462	2.391	1.581	2.030
^{6}FeOOH-1$_{rearr}$	2.631	2.030	1.452	2.410	1.618	2.086

[a] The left-hand superscript signifies the spin state of the species. [b] The H-bond between the proximal O and the carboxyl of Glu183. [c] The H-bond between the distal O and the carboxyl of Glu183. [d] The average value of the four Fe−N_{por} bond distances.

a TS **^{2}TS$_{OH}$-1** leading to a Cpd 0 intermediate **^{2}FeOOH-1** that has stability similar to that of **^{2}FeHOOH-1** (0.27 kcal/mol higher). In comparison, on the sextet state energy profile, a deprotonation barrier of 4.67 kcal/mol leads to the sextet state of Cpd 0 (**^{6}FeOOH-1**) that lies 4.79 kcal/mol higher than **^{6}FeHOOH-1**. However, the so-formed sextet Cpd 0 lies on a very flat potential and is expected to return easily back to **^{6}FeHOOH-1**.

The so-formed **^{2}FeOOH-1** and **^{6}FeOOH-1** species maintain H-bonding between the proximal O and Glu183. As shown in Figure 3, a subsequent conformational change rearranges the Cpd 0 intermediates to **^{2}FeOOH-1$_{rearr}$** and **^{6}FeOOH-1$_{rearr}$**, via **^{2}TS$_{OH}$-1$_{rearr}$** and **^{6}TS$_{OH}$-1$_{rearr}$**; in these rearranged conformations, Glu183 forms a H-bond with the distal O atom. The rearrangement barrier for the doublet Cpd 0 is low, 0.08 kcal/mol, and it is somewhat higher (3.08 kcal/mol) for the sextet state (see scan profiles in Figure S2 in the Supporting Information).

Unlike the doublet and sextet state mechanisms for the formation of Cpd 0, on the quartet surface, there is no local energy minimum for the **^{4}FeOOH-1** Cpd 0 species. An energy scan using the $O_{proximal}$-H bond distance as the deprotonation reaction coordinate, starting from **^{4}FeHOOH-1** (see Figure S3 in the Supporting Information) enabled us to estimate that the barrier for the quartet Cpd 0 intermediate **^{4}FeOOH-1$_{rearr}$**, in which Glu183 forms a H-bond with the distal O atom, is 10.15 kcal/mol (B2 datum).

The calculated relative energies and key geometric parameters for the five Cpd 0 species of CPO are collected in Figure 2 and Table 2, respectively. It can be seen that doublet Cpd 0 **^{2}FeOOH-1$_{rearr}$** is much lower in energy (by about 6−10 kcal/mol) than the other Cpd 0 species and that its generation from **^{2}FeHOOH-1** is also exothermic by 6.8 kcal/mol (which mean a serious reduction of $pK_a(H_2O_2)$ compared with that of the free molecule). This result, along with the calculated low barriers from **^{2}FeHOOH-1** to **^{2}FeOOH-1$_{rearr}$**, enables us to think that **^{2}FeOOH-1$_{rearr}$** is the most probable intermediate in Mechanism I toward the formation of CPO Cpd I. In summary, although the doublet state is not the lowest spin state of the Fe^{III}−HOOH species, it has the lowest energy transition state en route to Cpd 0. Therefore, the transformation process from Fe^{III}−HOOH to Cpd 0 is likely to take place on the doublet surface, preceded by a spin inversion from quartet to doublet (see Figure 2 above). We recall that the B3LYP functional has been found to exaggerate the stability of the quartet state of the resting state ($Fe^{III}-OH_2$) in P450cam[52] and to slightly underestimate the stability of the low spin state.[53] Since $Fe^{III}-OH_2$ and Fe^{III}−HOOH are quite similar, the possible overestimated stability of the quartet state here for Fe^{III}−HOOH is also expected, but there is no good way to quantify this in DFT. A small change in the relative energy would suggest that the doublet state should play an even more dominant role in Mechanism I of Cpd I formation in CPO.

3.1.3. O−O Activation and Conversion of Cpd 0 to Cpd I. Since **^{2}FeOOH-1$_{rearr}$** is significantly more stable than **^{2}FeOOH-1** (6.55 kcal/mol lower at the QM/MM B2 level), and since the transition between them is associated with a low barrier, **^{2}FeOOH-1$_{rearr}$** is the appropriate starting point for exploring the O−O activation process. Using the O−O bond distance as the reaction coordinate, we initially scanned the energy for the process (see Figure S4 in the Supporting Information). However, with this scan the calculation led to an artificial drop in energy. Our analysis of the energy drop showed that essentially the process involves the following main events: (i) a partial O−O homolytic cleavage, followed by (ii) proton coupled electron transfer (PCET) whereby Glu183 donates a proton to the departing OH radical, while at the same time, the Fe−O moiety transfers an electron to this departing OH radical, transforming the O−O cleavage to a heterolytic process and hence producing initially an unstable Fe(V) oxo intermediate **^{2}PorFe^{V}O** (electronic isomer of normal Cpd I), and (iii) electron transfer (ET) from the porphyrin ring to the Fe^VO moiety generates the ground-state Cpd I species, **^{2}Por$^{\bullet+}$Fe^{IV}O-1**. The first two processes (i) and (ii) occur jointly and the subsequent process (iii) transpires with very low energy cost of less than 0.5 kcal/mol at the QM/MM B1 level (see Figure S4 in the Supporting Information). In any event, to test whether the artificial energy drop in the formation of the unstable Fe^VO intermediate can be avoided, we performed a two-dimensional scan calculation using the O−O and O_{distal}-H distances as the reaction coordinates. As seen from Figure 4, the two-dimensional scan calculation that describes the O−O cleavage taking into account the possible protonation of the distal O atom enabled us to obtain a clear global picture of the O−O cleavage from the doublet Cpd 0 all the way to Cpd I (note that the conversion from **^{2}PorFe^{V}O** to Cpd I is virtually barrierless). We also obtained an O−O cleavage TS **^{2}TS$_{OOH}$** by full TS geometry optimization starting from a carefully chosen initial structure on the two-dimensional energy surface. The barrier for the O−O cleavage was found to be 12.38 kcal/mol (B2). The **^{2}TS$_{OOH}$** structure in Figure 4 exhibits an O−O bond distance of 1.816 Å (compared with 1.463 Å in Cpd 0 **^{2}FeOOH-1$_{rearr}$**) and an O_{distal}-H bond distance of 1.059 Å, indicating that the TS is much like a protonated Cpd 0 species. In fact, **^{2}TS$_{OOH}$** is quite similar to the corresponding O−O cleavage TS from Cpd 0 found in a recent QM/MM theoretical study on P450cam.[34] However, here the two-dimensional scan shows that there is no minimum existing as either a protonated Cpd 0 species or an OH radical in CPO on the doublet potential energy surface (PES).

In the so-produced Cpd I (**^{2}Por$^{\bullet+}$Fe^{IV}O-1**), continuing downward from the left most side of Figure 4, the water molecule H_2O_{distal} generated during the process is not yet in the most stable conformation. Subsequent calculations indicate (see Figure S5 in the Supporting Information) that **^{2}Por$^{\bullet+}$Fe^{IV}O-1** changes the conformation through TS **^{2}TS$_{FeO}$-**

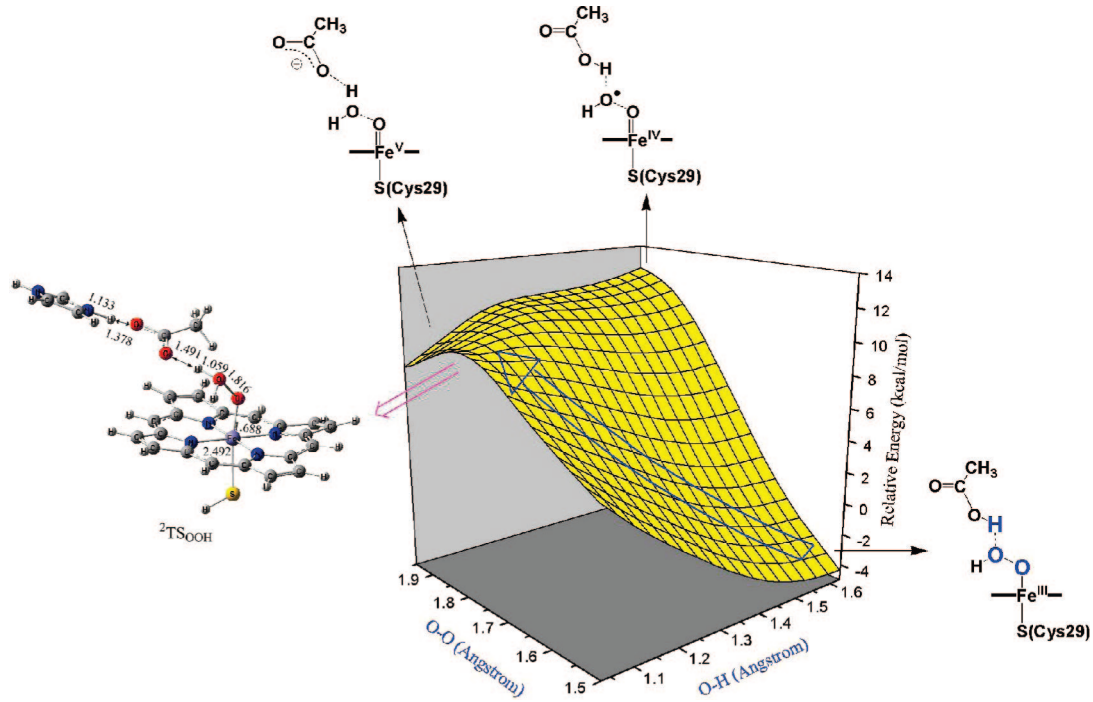

Figure 4. Two-dimensional PES scan starting from **^{2}FeOOH-1$_{rearr}$** using the O−O and O_{distal}−H distances as the reaction coordinates. Shown on the left-hand side is the structure of TS to the so-formed Cpd I species.

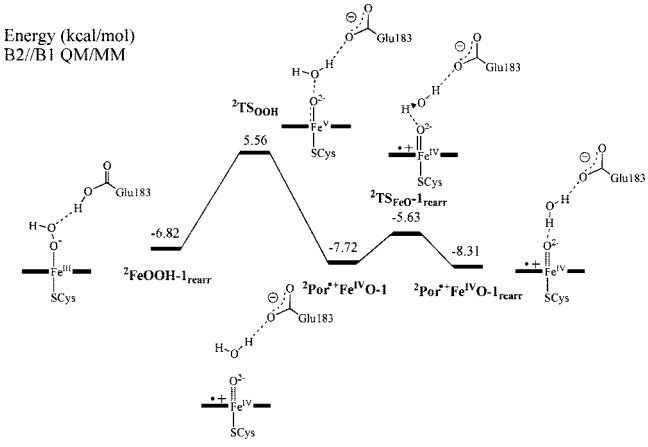

Figure 5. Energy profile (B2 value) for the O−O cleavage starting from **^{2}FeOOH-1$_{rearr}$** and the conformational rearrangement of the so-generated Cpd I.

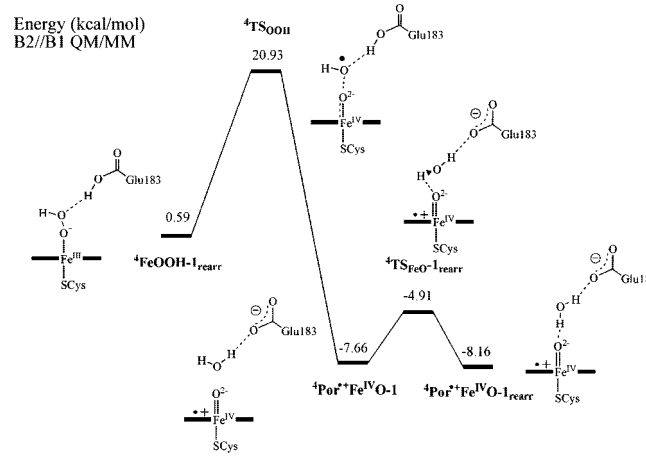

Figure 6. Energy profile (B2 value) for the O−O cleavage starting from **^{4}FeOOH-1$_{rearr}$** and the conformation rearrangement of the so-generated Cpd I.

1$_{rearr}$, to a slightly more stable conformation **^{2}Por$^{\bullet+}$Fe^{IV}O-1$_{rearr}$**, in which the water maintains one H-bond with the oxygen atom in the Fe═O unit. The barrier for this rearrangement of the water molecule is only 2.09 kcal/mol (B2). The catalytic role of this H-bonded water molecule was recently discussed in P450cam.[54] The O−O activation from Cpd 0 to generate Cpd I for the doublet state is summarized in Figure 5.

The O−O cleavage from Cpd 0 for the quartet state is shown in Figure 6. Here, in addition to the bond breaking, the electronic structure undergoes a major change (see below Scheme 4). This is the cause of the large barrier (20.34 kcal/mol at B2) shown in Figure 6, where the electronic configuration undergoes the requisite change through a transition structure, **^{4}TS$_{OOH}$**, at an O−O bond distance of 1.90 Å (see Figure S6 in the Supporting Information). The departing OH moiety, at an O−O bond distance exceeding 1.90 Å, possesses a single electron in a 2p orbital, thus confirming the homolytic manner of the O−O cleavage. Past the electronic configuration change, further increasing of the O−O bond length causes a decrease in energy with a subsequent proton transfer from Glu183 to the distal O atom, at an O−O bond distance of 2.10 Å. This proton transfer is attended by an electron transfer from porphyrin to the OH moiety completing the formation of the water molecule. Once again, a PCET mechanism is at work here leading finally to the normal configuration of the quartet Cpd I ^{4}Por$^{\bullet+}$Fe^{IV}═O species (**^{4}Por$^{\bullet+}$Fe^{IV}O-1**). Much like the mechanism for the doublet state, here (Figure 6) too, neither the OH radical species nor the protonated Cpd 0 is a genuine energy minimum in the process.

As already mentioned, there is a notable difference between the doublet state and the quartet state process in that prior to the PCET that forms Cpd I plus water, the quartet state complex must undergo a change in its electronic configuration, as illustrated in Scheme 4. Thus, initially Cpd 0 involves an open-shell configuration with one electron each in the π^*_{yz} and d_{xz} orbitals and in the high lying $\sigma^*_{z^2}$ orbital. During the elongation of the O−O bond, the FeO bond gets shorter, and this raises

SCHEME 4: Electronic Configuration Evolvement from Cpd 0 to Cpd I on the Quartet Surface

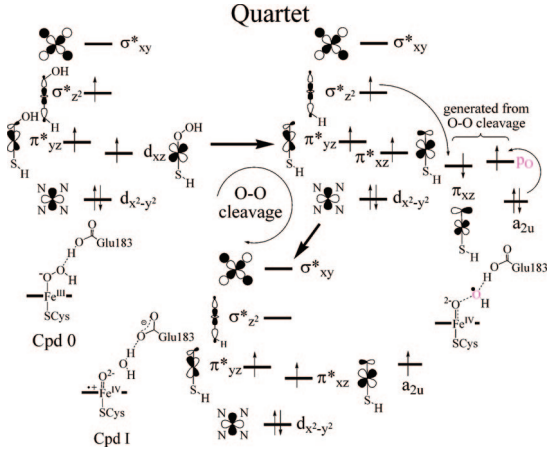

the energy of $\sigma^*_{z^2}$ but lowers the energy of Fe=O π orbitals. As a result, the electron in $\sigma^*_{z^2}$ is shifted to π (generated from homolytic O−O cleavage and having one electron) and forms one doubly occupied π orbital in Cpd I; this rearrangement is not required in the case for the doublet state process. Subsequently, much like in the doublet state, here too PCET takes place; as O−O elongation continues, an electron shifts from the porphyrin a_{2u} orbital to the singly occupied orbital of the OH radical, which becomes OH^- and gets protonated by Glu183. Again, much like the doublet process, in the so directly generated Cpd I species **^{4}Por$^{\bullet+}$Fe^{IV}O-1** in Figure 6, the water does not form a H-bond with the ferryl Fe=O unit. Thus, here too there is a conformational transition, with a small barrier of 2.75 kcal/mol (B2) (see Figure S7 in the Supporting Information) to relax Cpd I **^{4}Por$^{\bullet+}$Fe^{IV}O-1** to a slightly more stable one **^{4}Por$^{\bullet+}$Fe^{IV}O-1$_{rearr}$** having a H-bond between the water and O of the ferryl Fe=O unit.

We also performed an energy scan for the formation of Cpd I on the sextet surface, starting from **^{6}FeOOH-1$_{rearr}$** (see Figure S8 in the Supporting Information). A transition structure, **^{6}TS$_{OOH}$**, was located with a barrier of 24.1 kcal/mol high at the QM/MM B2 level. However, no Cpd I was formed after the O−O heterolytic cleavage and the proton transfer from Glu183 to the distal O atom. Instead, an N−O adduct product **^{6}FeON** (N-oxide) was formed whereby the ferryl FeO and one of the equatorial N atoms of porphyrin are bonded with an O−N bond distance of 1.411 Å. Such a species has been postulated during the reaction of Cpd I,[55] but has never been reported for the O−O cleavage process from doublet or quartet Cpd 0 of any heme-containing enzyme. The calculated energies (see Table S2 in the Supporting Information) indicate that **^{6}FeON** has stability similar to the doublet and quartet Cpd I species, namely, **^{2}Por$^{\bullet+}$Fe^{IV}O-1$_{rearr}$** and **^{4}Por$^{\bullet+}$Fe^{IV}O-1$_{rearr}$**. Since the N-oxide species such as **^{6}FeON** has apparently no oxidation activity,[55] its detailed study is out of the scope of the current study.

The energy calculations of the TSs **^{2}TS$_{OOH}$**, **^{4}TS$_{OOH}$**, and **^{6}TS$_{OOH}$** at the QM/MM B2 level indicate that **^{2}TS$_{OOH}$** is about 15 and 19 kcal/mol lower than **^{4}TS$_{OOH}$** and **^{6}TS$_{OOH}$**, respectively. Hence, one could exclude the possibility of the involvement of higher spin states (quartet and sextet) in Cpd I formation through Cpd 0 in CPO. These higher spin states will have to be formed from ^{2}Cpd I.

3.2. Mechanism II: Cpd I Formation Initiated by O−O Activation Directly from Fe^{III}−HOOH. Let us turn to inspect the results of the direct O−O activation from reactant Fe^{III}−HOOH.

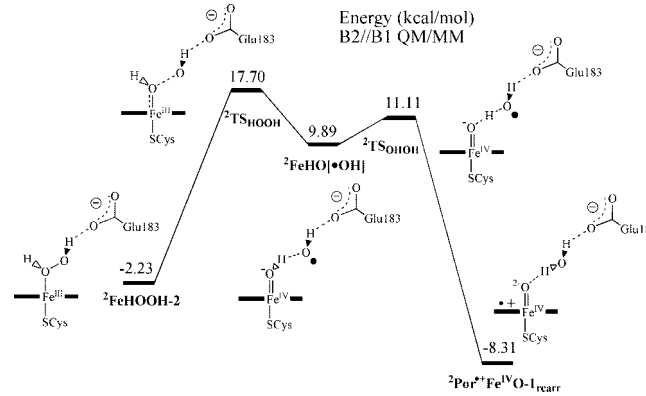

Figure 7. Energy profile from **^{2}FeHOOH-2** to Cpd I directly initiated by O−O activation. Relative energy data correspond to B2 (B1 data can be gleaned from Figure 2).

3.2.1. O−O Cleavage from Fe^{III}−HOOH. First, we scanned the PES from **^{2}FeHOOH-2** using the O−O bond distance as the reaction coordinate, and the energy profile is shown in Figure 7 (see Figure S9 in the Supporting Information).[56] The height of the calculated barrier for O−O cleavage is 19.9 kcal/mol (B2 datum), and the corresponding **^{2}TS$_{HOOH}$** species has an O−O bond distance of 2.06 Å. As a result of the homolytic O−O cleavage, a bound OH radical **^{2}FeHO[•OH]** is produced and found to be a genuine minimum unlike the corresponding state in Mechanism I. The calculated energy of **^{2}FeHO[•OH]** relative to **^{2}FeHOOH-2** is 12.1 kcal/mol (B2). The •OH moiety within **^{2}FeHO[•OH]** is H-bonded both to the carboxyl group of Glu183 and to the proximal OH moiety. The latter H-bond in **^{2}FeHO[•OH]** enables the •OH radical to abstract a hydrogen atom from the proximal OH and thereby form Cpd I, which will be discussed in detail in the next section.

Similar scan calculations were performed for the quartet and sextet states, using the O−O bond distance as the reaction coordinate (see Figures S11 and S12 in the Supporting Information). These calculations led to corresponding transition state species, **^{4}TS$_{HOOH}$** and **^{6}TS$_{HOOH}$**, with barriers of 29.3 and 29.0 kcal/mol, respectively (B2 data). The O−O bond distances in **^{4}TS$_{HOOH}$** and **^{6}TS$_{HOOH}$** are 2.00 and 1.98 Å, respectively, and these values are similar to the corresponding one for the double state. The energies of the produced OH radical species, **^{4}Fe^{IV}HO[•OH]** and **^{6}Fe^{IV}HO[•OH]**, relative to the corresponding reactant Fe^{III}−HOOH are 15.5 and 23.7 kcal/mol (B2), respectively. Considering that the relative energies of **^{2}FeHOOH-2**, **^{4}FeHOOH-2**, and **^{6}FeHOOH-2** are −2.23, −6.03, and −3.16 kcal/mol, respectively, we can conclude that although the O−O bond activation of the Fe^{III}−HOOH species encounters significant barriers, the bond cleavage process is slightly more facile for the doublet state than for the other two spin states (the activation energy for O−O cleavage for the doublet state is 23.7 kcal/mol after considering the transition from the ground state **^{4}FeHOOH-2** to **^{2}FeHOOH-2**), which is same as the relative ease noted for Mechanism I (see Figure 2). We note that by contrast to these high O−O cleavage barriers in CPO, our calculations for the enzyme HO yielded much lower barriers for the O−O cleavage (11 kcal/mol) of the corresponding Fe^{III}−HOOH complexes.[37]

3.2.2. PCET from the OH Radical to Form Cpd I during Mechanism II. We have shown above that O−O cleavage from Fe^{III}−HOOH generates the bound •OH radical species, **^{2}Fe^{IV}HO[•OH]**, **^{4}Fe^{IV}HO[•OH]**, and **^{6}Fe^{IV}HO[•OH]**. The •OH radicals in these three intermediates are held by H-bonds, with the proximal OH group (through H on the proximal O) therefore

TABLE 3: Key Bond Distance *R* (in Å) of the Three Spin States of Cpd I[a]

	R (Fe−S)	*R* (Fe−O)	*R* (O−O)	R (O_{prox}−H)[b]	R_{av} (Fe−N_{por})[c]
^{2}Por$^{\bullet+}$Fe^{IV}O-1	2.589	1.614	2.731	3.665	2.033
^{4}Por$^{\bullet+}$Fe^{IV}O-1	2.580	1.614	2.732	3.650	2.033
^{2}Por$^{\bullet+}$Fe^{IV}O-1$_{rearr}$	2.559	1.618	2.758	1.790	2.033
^{4}Por$^{\bullet+}$Fe^{IV}O-1$_{rearr}$	2.553	1.619	2.769	1.799	2.033
^{6}Por$^{\bullet+}$Fe^{IV}O-1$_{rearr}$	2.524	1.621	2.757	1.795	2.094

[a] The left-hand superscript signifies the spin state of the species. [b] The H-bond between the proximal O and the produced water. [c] The average value of the four Fe−N_{por} bond distances.

TABLE 4: Spin Distribution of the Three Spin States of Cpd I at the QM/MM B2 Level[a]

	Fe	$O_{proximal}$	S	porphyrin	Glu183+ His105	H_2O[b]
^{2}Por$^{\bullet+}$Fe^{IV}O-1	1.30	0.90	−0.14	−1.06	0.00	0.00
^{4}Por$^{\bullet+}$Fe^{IV}O-1	1.14	0.93	0.12	0.80	0.00	0.00
^{2}Por$^{\bullet+}$Fe^{IV}O-1$_{rearr}$	1.38	0.83	−0.13	−1.09	0.00	0.00
^{4}Por$^{\bullet+}$Fe^{IV}O-1$_{rearr}$	1.21	0.86	0.10	0.83	0.00	0.01
^{6}Por$^{\bullet+}$Fe^{IV}O-1$_{rearr}$	3.13	0.65	0.03	1.18	0.00	0.00

[a] The left-hand superscript signifies the spin state of the species. [b] The water molecule generated from the distal O atom.

generating suitable conformations for the hydrogen abstraction reaction from the proximal O atom to the distal •OH moiety. Using the O_{distal}−$H_{proximal}$ distance as the reaction coordinate, we scanned the energy profiles for hydrogen abstraction from the proximal OH by the •OH radical, in **^{2}Fe^{IV}HO[•OH]**, **^{4}Fe^{IV}HO[•OH]**, and **^{6}Fe^{IV}HO[•OH]**. The result for the doublet state is shown in Figure 7, while others are shown in the Supporting Information (see Figures S13−S15). From the scans passing through transition structures **^{2}TS$_{OHOH}$**, **^{4}TS$_{OHOH}$**, and **^{6}TS$_{OHOH}$**, the hydrogen abstraction barriers for these three states were estimated to be extremely small: 1.2, 1.3, and 2.3 kcal/mol, respectively (B2 data). Although the process is formally a hydrogen atom transfer, mechanistically it occurs by PCET, namely, a proton transfer to OH• and a concomitant electron transfer from the porphyrin a_{2u}-type orbital to the OH moiety, as discussed above for Mechanism I (see, e.g., the electron transfer in Scheme 4).

An additional interesting feature is that unlike Mechanism I, here the Cpd I **^{2}Por$^{\bullet+}$Fe^{IV}O-1$_{rearr}$**, **^{4}Por$^{\bullet+}$Fe^{IV}O-1$_{rearr}$**, and **^{6}Por$^{\bullet+}$Fe^{IV}O-1$_{rearr}$** species are generated directly with a H-bond between the ferryl Fe═O unit and the produced water. The calculated energies, geometries, and spin distribution for all Cpd I species found in this study are summarized in Figure 2 and Tables 3 and 4. One can see that the doublet and quartet Cpd I species are almost degenerate in energy, which can be expected since they are triradicaloid species. However, as found before in P450cam,[51] here too the sextet Cpd I, which is pentaradicaloid with additional unpaired electrons in the $d_{x^2-y^2}$ and σ^*_{xy} orbitals, lies about 10 kcal/mol (B2) higher in energy than the doublet and quartet species. Incidentally, the **^{2}PorFe^{V}O** electromer lies at about the same energy as the sextet state species.

4. Discussion

4.1. Formation of Cpd 0. According to our calculations, the transformation from Fe^{III}−HOOH to Cpd 0, by proton transfer from the proximal O to Glu183, is extremely facile especially via the doublet state process, where the barrier is only 1.55 kcal/mol (Figure 2). Even after accounting for the fact that the relative energy of **^{2}FeHOOH-1** is 4.55 kcal/mol higher than

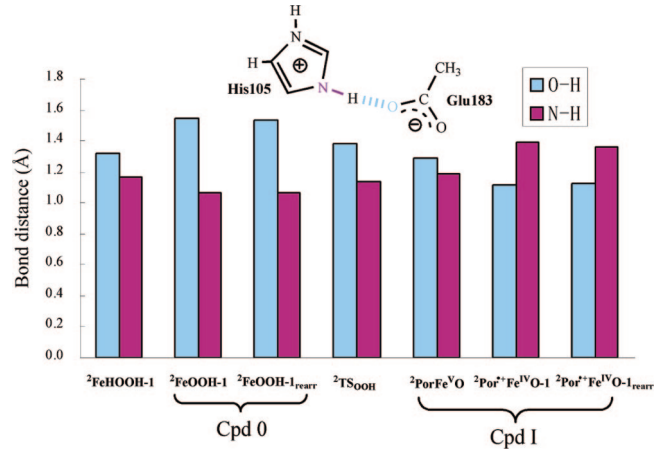

Figure 8. Evolution of the N−H (violet) and H−O (blue) distances of the shared proton between Glu183 and His105 along the reaction processes from reactant **^{2}FeHOOH-1** to product Cpd I.

the quartet ground state, the total activation energy is just 6.1 kcal/mol. Of course, the spin-crossover from the quartet ground state to the doublet state in Figure 2 is expected to be facile too, since the spin−orbit coupling (SOC) between the two states is quite large.[57] In contrast, the direct O−O cleavage from Fe^{III}−HOOH involves much higher activation energies of at least 20 kcal/mol. Therefore, in CPO, starting from Fe^{III}−HOOH, the predominant reaction pathway will be Mechanism I, which proceeds via Cpd 0.

Interestingly, by comparison to the Cpd I formation in horseradish peroxidase, HRP, Mechanism I for CPO is simpler and more straightforward. Thus, the recent QM/MM treatment of HRP demonstrated that the deprotonation of Fe^{III}−HOOH to yield Cpd 0 has a high barrier of about 20 kcal/mol unless a water molecule that is attached to Pro139 can migrate to bridge the His42 and the Fe^{III}−HOOH moiety to thereby facilitate the proton transfer from H_2O_2 to the distal residue His42. With the bridging water molecule, the deprotonation barrier dropped to 5.72 kcal/mol at a QM/MM level comparable with that adopted in the current study.[36] As shown above (Figure 1), in the case of CPO, the distal residue Glu183 is ideally located to accept a proton from the Fe^{III}−HOOH moiety, without the need for any bridging water assistance.

Another interesting comparison is the spin-state energy gap for Cpd 0 in CPO vis-à-vis P450cam. In CPO, the calculated QM/MM energy gap of the doublet and quartet states (7.4 kcal/mol, B2 datum in Figure 2) is smaller than that for P450cam (13−14 kcal/mol).[34] In fact, the calculated doublet−quartet gap without the protein environment (the QM part gas phase calculation at the QM/MM optimized geometry) is 11.2 kcal/mol (B2 datum). Comparing with the doublet−quartet gap of 5.0 kcal/mol from the QM energy part of QM/MM B2 calculation (see the Supporting Information), it can be seen that through polarization, the protein environment decreases the doublet−quartet adiabatic gap by 6.2 kcal/mol in CPO. This may reflect the stabilization of the $\sigma^*_{z^2}$ orbital by the more polar CPO environment compared with P450cam.[59] As has been shown by Thiel et al.,[52] the main factor of stabilizing the quartet state within the enzyme environment is the bulk polarity that lowers the singly occupied $\sigma^*_{z^2}$ orbital. Our calculation indicates that the energy gap between the d_{xz} and $\sigma^*_{z^2}$ orbitals (the occupied α-spin Kohn−Sham orbital) is decreased from 4.98 eV in the gas phase (QM/MM geometry) to 4.56 eV in the enzyme. This conforms with the previous findings that the protein environment stabilizes the quartet state compared to the doublet state.[52]

SCHEME 5: Summarized Mechanisms for O−O Activation in Heme-Containing Enzymes P450cam, HRP, CPO, HO, and NOS from QM/MM Theoretical Studies[a]

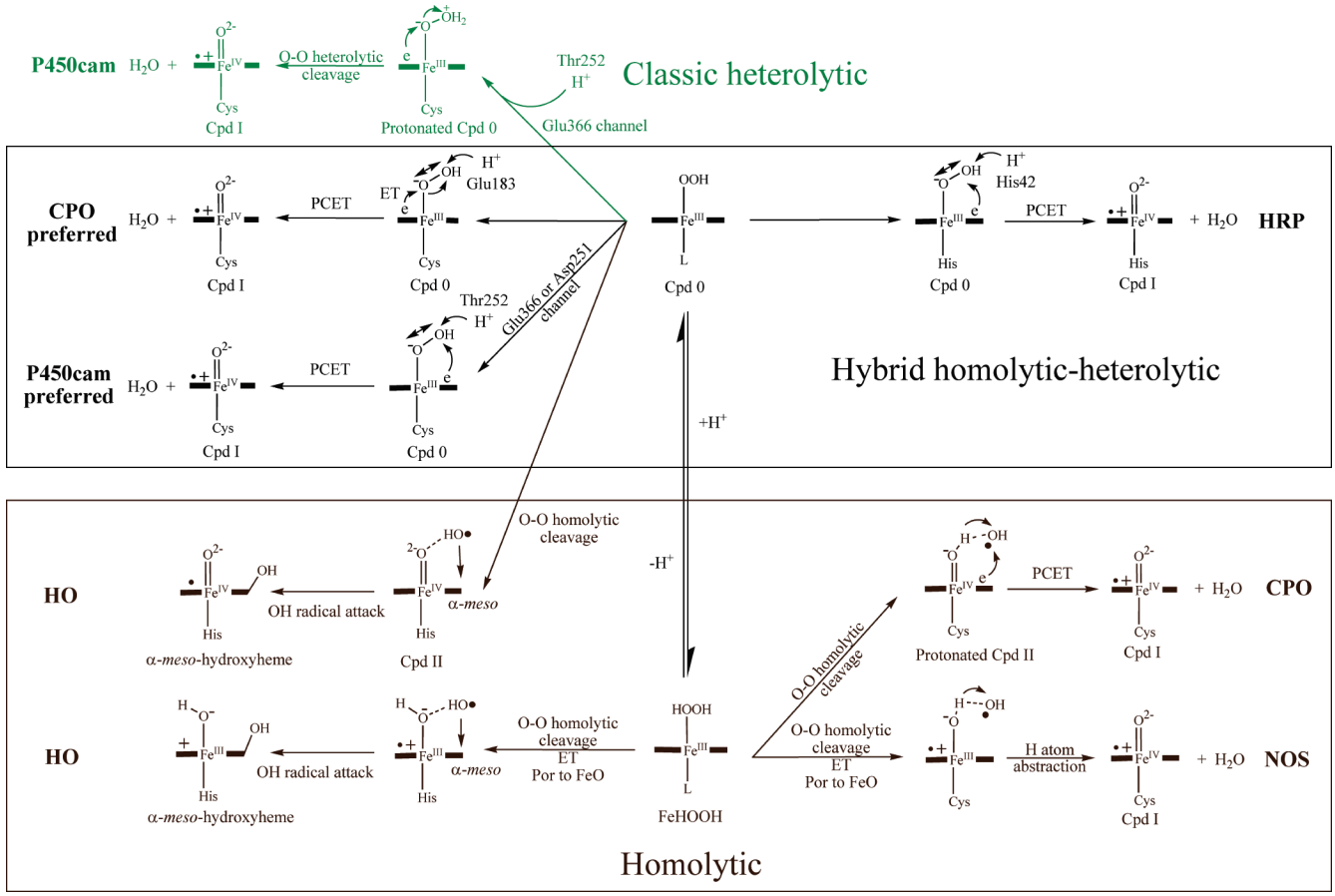

[a] The O−O activation started from Cpd 0 in the study of P450cam.[34] For CPO, NOS,[35] and HRP[36] it started from Fe^{III}−HOOH. In the study of HO, the O−O activation was explored for both Cpd 0 and Fe^{III}−HOOH species.

4.2. Potential Function of His105. It has been postulated[28] that His105 functions primarily to fix Glu183 and to modulate its acidity. The first point is quite clear because through H-bond interaction, Glu183 always keeps close to His105 along the whole reaction process of Cpd I formation. In order to elucidate the second point, we show in Figure 8 the evolvement of the NH and OH bond/H-bond distances along the energetically most preferred pathway of Cpd I formation in CPO (Mechanism I above).[60] One can see quite clearly how these two bonds evolve along the reaction processes from Fe^{III}−HOOH toward Cpd I, through which the acidity of Glu183 is adjusted. The general propensity shown in Figure 8 is that in fact His105 is relaying its proton to Glu183 as the formation of Cpd I progresses. As such, His105 adjusts the acidity of Glu183, as postulated before.[28]

4.3. Protonated Cpd 0. The protonated Cpd 0, Fe^{III}−OOH_2 has been characterized as a local energy minimum in a recent QM/MM study of Cpd I formation in P450cam.[34] Thus, in one of the protonation channels (via Glu366), this species was found to be a genuine minimum, with an O−O bond distance of 1.558 Å, and to lie 33.1−41.1 kcal/mol higher than Cpd 0, depending on the basis set used. From this high-energy protonated Cpd 0 minimum in P450cam, a subsequent O−O cleavage TS was located with an O−O bond distance of 1.813 Å and with a low barrier of 4 kcal/mol. In the present case of CPO (see Figure 4) as well as in HRP,[36] protonated Cpd 0 is not an energy minimum throughout the O−O distance variation. However, in CPO the O−O cleavage TS ($^2TS_{OOH}$) resembles a protonated Cpd 0 species. The relative energy (about 12.4 kcal/mol) of this TS to the proceeding Cpd 0 is much lower than in the case of P450cam, thereby favoring the pathway through $^2TS_{OOH}$ in the transformation of Cpd 0 to Cpd I in CPO.

4.4. Issue of Homolytic versus Heterolytic O−O Cleavage in Heme Enzymes. By now, the O−O activation mechanism has been studied in several heme-containing enzymes, i.e., P450cam, HRP, HO, and NOS, by means of QM/MM calculation. Two preferred mechanistic types were found: (i) a homolytic O−O cleavage as in HO,[37] NOS[35] and (ii) a heterolytic O−O cleavage (including classic heterolytic and hybrid homolytic-heterolytic) as in CPO, HRP,[36] and P450cam.[34] These mechanisms are summarized in Scheme 5. Thus, the classical heterolytic O−O cleavage (induced by initial protonation of the distal oxygen of Cpd 0 and subsequent expulsion of H_2O) was found so far only in P450, where it occurs only via the Glu360 channel, and its barrier is too high to count as a realistic mechanism. In HRP[36] and CPO, Cpd I formation through Cpd 0 occurs through a concerted, albeit nonsynchronous, heterolytic cleavage, whereby the incipient OH radical moiety forms a water molecule in a barrier free fashion. Similarly, in P450cam also, the ultimately preferred mechanism was found to be a concerted but nonsynchronous hybrid homolytic−heterolytic process (when the larger basis set or QM region was used[34]). In the HO, NOS, and CPO reactions that proceed directly from the Fe^{III}−HOOH species, the mechanism is stepwise, involving initial homolytic O−O cleavage with subsequent processes of PCET in CPO, hydrogen abstraction in NOS,[35] and OH radical attack on heme in HO. Notably, the barriers in all these concerted or hybrid homolytic−heterolytic processes are significantly lower than in the genuine homolytic

process (where no electron transfer occurs from porphyrin to the proximal O) as in the direct CPO mechanism for $Fe^{III}-HOOH$ or as calculated in model systems.[61]

One interesting comparison is between the direct mechanisms of CPO and HO,[37] starting from the $Fe^{III}-HOOH$ complexes. Thus, in both cases, the mechanism involves initial O−O bond homolyses. (In CPO, this is followed by PCET to form Cpd I, and in HO it is followed by hydroxylating the *meso* position of the heme.) Nevertheless, the barriers are very different, being about 20 kcal/mol in CPO versus 11 kcal/mol in HO. Thus, as discussed before,[37] in the HO enzyme, where the O−O cleavage is attended by an electron transfer from porphyrin to the proximal O, the sizable water cluster near the Fe(HOOH) moiety as well as protein environment both stabilize the $Por^{\bullet+}Fe^{III}OH/[OH\bullet]$ intermediate, and thereby strongly favor O−O homolysis. This cluster is absent in CPO, and therefore, the direct $Fe^{III}-HOOH$ channel is silent.

4.5. Relative Energies of Cpd I and Cpd 0. The energy of Cpd I relative to Cpd 0 is important because it serves as an index of stability of Cpd I. From our calculation on the QM/MM B2 level, the most stable Cpd I (^{2}**Por$^{\bullet+}$Fe^{IV}O-1$_{rearr}$**) is about 1.5 kcal/mol lower than the most stable Cpd 0 (^{2}**FeOOH-1$_{rearr}$**). Thus, these two species are comparable in energy. Likewise, QM/MM calculations of P450cam Cpd I, with several different QM regions and basis sets, indicated the Cpd I is of energy similar to that of Cpd 0.[34] In HRP, however, Cpd I is calculated to be about 27 kcal/mol more stable than Cpd 0.[36] This is consistent with the experimental fact that Cpd I of HRP is isolable. The relative stability of Cpd I in CPO and P450 does not explain, however, why Cpd I can be probed in the native cycle of CPO but is too short lived for detection in the native cycle of P450cam.

As shown in Figure 2, our QM/MM calculations for Cpd I reproduce the doublet ground state known from experiment.[23] The exchange coupling constant J is a measure of the interaction between the radical on $Por^{\bullet+}$ and the triplet configuration in the ferryl $Fe^{IV}=O$ unit. Our calculated value for the most stable quartet and doublet Cpd I here (^{2}**Por$^{\bullet+}$Fe^{IV}O-1$_{rearr}$** and ^{4}**Por$^{\bullet+}$Fe^{IV}O-1$_{rearr}$**) is -51 cm^{-1} at the QM/MM B2 level, which is in very good agreement with the experimental value of -58 cm^{-1}.[23,62,63] In addition, the recent experiment shows that in Cpd I of CPO, the maximum value for the sulfur (Cys29) spin density is maximum 0.23.[62] This result is consistent with the current QM/MM calculation of 0.10−0.12 (Table 4) but does not agree with QM model calculations in the gas phase, which predict that most of the spin density should reside on the sulfur.[65,66] As already explained[25d,67] and further demonstrated by QM/MM calculation,[68] the spin density is small because of the bulk polarity effects and the amidic H-bonds to sulfur (from Ala31 and Leu32). Here, the calculated third unpaired electron for doublet and quartet Cpd I of CPO is in the porphyrin a_{2u} orbital. This agrees with previous QM/MM studies of P450cam,[51a,68] HRP,[69] and CAT[38] but differs from those of cytochrome *c* peroxidase (CCP)[70] and catalase-peroxidase (KatG),[71] where the third unpaired electron is located on a protein residue.

5. Conclusions

This work constitutes a systematic study of the Cpd I formation mechanism in CPO by means of QM/MM calculations. Two possible pathways starting from $Fe^{III}-HOOH$ were examined on the doublet, quartet, and sextet energy surfaces. The calculations showed that the most preferred pathway for the formation of CPO Cpd I is the one proceeding on the doublet surface in the following manner: $Fe^{III}-HOOH \rightarrow$ Cpd 0 → Cpd I. The corresponding barrier for the rate-limiting step (O−O cleavage from Cpd 0) is about 12.4 kcal/mol at the QM/MM B2 level. Compared with this path, the one initiated by a direct O−O cleavage from $Fe^{III}-HOOH$ is less favorable, having an activation energy of at least 23.7 kcal/mol.

Proton coupled electron transfer (PCET) was found to play an important role in the O−O cleavage and the formation of Cpd I. Before the proton transfer to the distal O atom, the O−O cleavage from Cpd 0 tends to occur in a homolytic fashion, but the proton transfer triggers an electron transfer from the proximal O atom (change the O−O cleavage to be heterolytic) or the porphyrin ring to the incipient water molecule. This feature resembles the recent mechanisms found by QM/MM analysis for P450cam[34] and HRP.[36] In all cases, PCET lowers the O−O cleavage barrier below the corresponding one of a purely homolytic cleavage.

Acknowledgment. Dedicated to T. Ziegler on the occasion of his forthcoming 65th Birthday. Tom Ziegler is highly appreciated for his contributions to quantum chemistry. This research is supported by the Israel Science Foundation (ISF) grant (to S.S.) and the Deutsche Forschungsgemeinschaft Grant SFB 623 (to I.S.). H.C. thanks the Golda Meir fellowship fund. H.H. is a JSPS Postdoctoral Fellow for Research Abroad. E.D. acknowledges the assistance of M. Warchol.

Supporting Information Available: Computational procedures, scan profiles, *xyz* coordinates, energies, spin and charge population of the various species, and complete refs 39 and 43. This material is available free of charge via the Internet at http://pubs.acs.org.

References and Notes

(1) Morris, D. R.; Hager, L. P. *J. Biol. Chem.* **1966**, *241*, 1763.
(2) Dawson, J. H.; Sono, M. *Chem. Rev.* **1987**, *87*, 1255.
(3) Woggon, W. D. *Top. Curr. Chem.* **1997**, *184*, 39.
(4) (a) Shaw, P. D.; Hager, L. P. *J. Am. Chem. Soc.* **1959**, *81*, 1101. (b) Beckwith, J. R.; Hager, L. P. *J. Biol. Chem.* **1963**, *238*, 3091.
(5) Geigert, J.; Neidleman, S. L.; Dalietos, D. J.; Dewitt, S. K. *Appl. Environ. Microbiol.* **1983**, *45*, 1575.
(6) Geigert, J.; Neidleman, S. L.; Dalietos, D. J. *J. Biol. Chem.* **1983**, *258*, 2273.
(7) (a) Hager, L. P.; Morris, D. R.; Brown, F. S.; Eberwein, H. *J. Biol. Chem.* **1966**, *241*, 1769. (b) Brown, F. S.; Hager, L. P. *J. Am. Chem. Soc.* **1967**, *89*, 719. (c) Morris, D. R.; Hager, L. P. *J. Biol. Chem.* **1966**, *241*, 3582. (d) Corbett, M. D.; Chipko, B. R.; Batchelor, A. O. *Biochem. J.* **1980**, *241*, 893.
(8) (a) Osborne, R. L.; Raner, G. M.; Hager, L. P.; Dawson, J. H. *J. Am. Chem. Soc.* **2006**, *128*, 1036. (b) Osborne, R. L.; Coggins, M. K.; Terner, J.; Dawson, J. H. *J. Am. Chem. Soc.* **2007**, *129*, 14838.
(9) (a) Cramer, S. P.; Dawson, J. H.; Hodgson, K. O.; Hager, L. P. *J. Am. Chem. Soc.* **1978**, *100*, 7282. (b) Blanke, S. R.; Hager, L. P. *J. Biol. Chem.* **1988**, *263*, 18739. (c) Dawson, J. H.; Holm, R. H.; Trudell, J. R.; Barth, G.; Linder, R. E.; Bunnenberg, E.; Djerassi, C.; Chiang, R.; Hager, L. P. *J. Am. Chem. Soc.* **1976**, *98*, 3709. (d) Dawson, J. H.; Kau, L.-S.; Penner-Hahn, J. E.; Sono, M.; Eble, K. S.; Bruce, G. S.; Hager, L. P.; Hodgson, K. O. *J. Am. Chem. Soc.* **1986**, *108*, 8114. (e) Dawson, J. H. *Science* **1988**, *240*, 433. (f) Sundaramoorthy, M.; Mauro, J. M.; Sullivan, A.; Terner, J.; Poulos, T. L. *Acta Crystallogr.* **1995**, *D51*, 842. (g) Sundaramoorthy, M.; Terner, J.; Poulos, T. L. *Structure* **1995**, *3*, 1367.
(10) Sono, M.; Roach, M. P.; Coulter, E. D.; Dawson, J. H. *Chem. Rev.* **1996**, *96*, 2841.
(11) (a) Groves, J. T.; Wang, C. C. Y. *Curr. Opin. Chem. Biol.* **2000**, *4*, 687. (b) Rosen, G. M.; Tsai, P.; Pou, S. *Chem. Rev.* **2002**, *102*, 1191.
(12) (a) Kedderis, G. L.; Koop, D. R.; Hollenberg, P. F. *J. Biol. Chem.* **1980**, *255*, 10174. (b) Kedderis, G. L.; Hollenberg, P. F. *J. Biol. Chem.* **1984**, *259*, 3663. (c) Ketters, G. L.; Hollenberg, P. F. *Arch. Biochem. Biophys.* **1984**, *233*, 315. (d) Okazaki, O.; Guengerich, F. P. *J. Biol. Chem.* **1993**, *268*, 1546.
(13) Zaks, A.; Dodds, D. R. *J. Am. Chem. Soc.* **1995**, *117*, 10419.
(14) (a) Hu, S.; Hager, L. P. *Biochem. Biophys. Res. Commun.* **1998**, *253*, 544. (b) Hu, S.; Hager, L. P. *J. Am. Chem. Soc.* **1999**, *121*, 872.

(15) (a) Allain, E. J.; Hager, L. P.; Deng, L.; Jacobson, E. N. *J. Am. Chem. Soc.* **1993**, *115*, 4415. (b) Colonna, S.; Gaggero, N.; Casella, L.; Carrea, G.; Pasta, P. *Tetrahedron: Asymmetry* **1993**, *4*, 1325. (c) Dexter, A. F.; Hager, L. P. *J. Am. Chem. Soc.* **1995**, *117*, 817. (d) Dexter, A. F.; Lakner, F. J.; Campbell, R. A.; Hager, L. P. *J. Am. Chem. Soc.* **1995**, *117*, 6412. (e) Hu, S.; Hager, L. P. *Tetrahedron Lett.* **1999**, *40*, 1641. (f) Lakner, F. J.; Hager, L. P. *J. Org. Chem.* **1996**, *61*, 3923. (g) Lakner, F. J.; Cain, K. P.; Hager, L. P. *J. Am. Chem. Soc.* **1997**, *119*, 443. (h) Lakner, F. J.; Hager, L. P. *Tetrahedron: Asymmetry* **1997**, *8*, 3547.

(16) (a) Colonna, S.; Gaggero, N.; Manfredi, A.; Casella, L.; Gullotti, M.; Carrea, G.; Pasta, P. *Biochemistry* **1990**, *29*, 10465. (b) Colonna, S.; Nicoletta, G.; Casella, L.; Carrea, G.; Pasta, P. *Tetrahedron: Asymmetry* **1992**, *3*, 95. (c) Casella, L.; Gullotti, M.; Ghezzi, R.; Berlinghelli, T.; Colonna, S.; Carrea, G. *Biochemistry* **1992**, *31*, 9451. (d) Fu, H.; Kondo, H.; Ichikawa, Y.; Look, G. C.; Wong, C.-H. *J. Org. Chem.* **1992**, *57*, 7265. (e) Doerge, D. R. *Arch. Biochem. Biophys.* **1986**, *244*, 678. (f) Kobayashi, S.; Nakano, M.; Goto, T.; Kimura, T.; Schapp, A. P. *Biochem. Biophys. Res. Commun.* **1986**, *135*, 166. (g) Alvarez, J. C.; Ortiz de Montellano, P. R. *Biochemistry* **1992**, *31*, 8315. (h) Allenmark, S. G.; Andersson, M. A. *Tetrahedron: Asymmetry* **1996**, *7*, 1089.

(17) (a) Doerge, D. R.; Corbett, M. D. *Chem. Res. Toxicol.* **1991**, *4*, 556. (b) Corbett, M. D.; Chipko, B. R.; Batchelor, A. O. *Biochem. J.* **1980**, *187*, 893.

(18) (a) Thomas, J. A.; Morris, D. R.; Hager, L. P. *J. Biol. Chem.* **1970**, *245*, 3129. (b) Casella, L.; Poli, S.; Gullotti, M.; Selvaggini, C.; Berlinghelli, T.; Marchesini, A. *Biochemistry* **1994**, *33*, 6377.

(19) Geigert, J.; Dalietos, D. J.; Neidleman, S. L.; Lee, T. D.; Wadsworth, J. *Biochem. Biophys. Res. Commun.* **1983**, *114*, 1104.

(20) Hager, L. P.; Doubek, D. L.; Silverstein, R. M.; Hargis, J. H.; Martin, J. C. *J. Am. Chem. Soc.* **1972**, *94*, 4364.

(21) Palcic, M. M.; Rutter, R.; Araiso, T.; Hager, L. P.; Dunford, H. B. *Biochem. Biophys. Res. Commun.* **1980**, *94*, 1123.

(22) (a) Egawa, T.; Proshlyakov, D. A.; Miki, H.; Makino, R.; Ogura, T.; Kitagawa, T.; Ishimura, Y. *J. Biol. Inorg. Chem.* **2001**, *6*, 46. (b) Hosten, C. M.; Sullivan, A. M.; Palaniappan, V.; Fitzgerald, M. M.; Terner, J. *J. Biol. Chem.* **1994**, *269*, 13966.

(23) Rutter, R.; Hager, L. P.; Dhonau, H.; Hendrich, M.; Valentine, M.; Debrunner, P. *Biochemistry* **1984**, *23*, 6809.

(24) (a) Hollenberg, P. F.; Hager, L. P. *J. Biol. Chem.* **1973**, *248*, 2630. (b) Hollenberg, P. F.; Hager, L. P. *J. Biol. Chem.* **1980**, *255*, 4801. (c) Chiang, R.; Makino, R.; Spomer, W. E.; Hager, L. P. *Biochemistry* **1975**, *14*, 4166. (d) Champion, P. M.; Munck, E.; Debrunner, P. G.; Hollenberg, P. F.; Hager, L. P. *Biochemistry* **1973**, *12*, 426. (e) Champion, P. M.; Chiang, R.; Munck, E.; Debrunner, P. G.; Hager, L. P. *Biochemistry* **1975**, *14*, 4159. (f) Bangcharoenpaurpong, O.; Champion, P. M.; Hall, K. S.; Hager, L. P. *Biochemistry* **1986**, *25*, 2374. (g) Fann, Y.-C.; Gerber, N. C.; Osmulski, P. A.; Hager, L. P.; Sligar, S. G.; Hoffman, B. M. *J. Am. Chem. Soc.* **1994**, *116*, 5989. (h) Hu, S.; Kincaid, J. R. *J. Biol. Chem.* **1993**, *268*, 6189. (i) Kellner, D. G.; Hung, S.-C.; Weiss, K. E.; Sligar, S. G. *J. Biol. Chem.* **2002**, *277*, 9641.

(25) (a) Denisov, I. G.; Makris, T. M.; Sligar, S. G.; Schlichting, I. *Chem. Rev* **2005**, *105*, 2253. (b) Meunier, B.; de Visser, S. P.; Shaik, S. *Chem. Rev.* **2004**, *104*, 3947. (c) Shaik, S.; Kumar, D.; de Visser, S. P.; Altun, A.; Thiel, W. *Chem. Rev.* **2005**, *105*, 2279. (d) Shaik, S.; Hirao, H.; Kumar, D. *Nat. Prod. Rep.* **2007**, *24*, 533.

(26) (a) Sono, M.; Dawson, J. H.; Hall, K.; Hager, L. P. *Biochemistry* **1986**, *25*, 347. (b) Dugad, L. B.; Wang, X.; Wang, C.-C.; Lukat, G. S.; Goff, H. M. *Biochemistry* **1992**, *31*, 1651. (c) Blanke, S. R.; Hager, L. P. *J. Biol. Chem.* **1990**, *265*, 12454.

(27) Poulos, T. L.; Kraut, J. *J. Biol. Chem.* **1980**, *255*, 8199.

(28) Sundaramoorthy, M. Chloroperoxidase. In *Handbook of Metalloproteins*; Messerschmidt, A., Huber, R., Poulos, T. L., Wieghardt, K., Eds.; John-Wiley and Sons; New York, 2001, Vol. 1, pp 233−244.

(29) Yi, X. W.; Conesa, A.; Punt, P. J.; Hager, L. P. *J. Biol. Chem.* **2003**, *278*, 13855.

(30) Sundaramoorthy, M.; Terner, J.; Poulos, T. L. *Chem. Biol.* **1998**, *5*, 461.

(31) Filizola, M.; Loew, G. H. *J. Am. Chem. Soc.* **2000**, *122*, 3599.

(32) (a) Senn, H. M.; Thiel, W. *Top. Curr. Chem.* **2007**, *268*, 173. (b) Senn, H. M.; Thiel, W. *Curr. Opin. Chem. Biol.* **2007**, *11*, 182. (c) Lin, H.; Truhlar, D. G. *Theor. Chem. Acc.* **2007**, *117*, 185.

(33) Decker, A.; Solomon, E. I. *Curr. Opin. Chem. Biol.* **2005**, *9*, 152.

(34) Zheng, J. J.; Wang, D. Q.; Thiel, W.; Shaik, S. *J. Am. Chem. Soc.* **2006**, *128*, 13204.

(35) Cho, K.-B.; Derat, E.; Shaik, S. *J. Am. Chem. Soc.* **2007**, *129*, 3182.

(36) (a) Derat, E.; Shaik, S. *J. Phys. Chem. B* **2006**, *110*, 10526. (b) Derat, E.; Shaik, S.; Rovira, C.; Vidossich, P.; Alfonso-Prieto, M. *J. Am. Chem. Soc.* **2007**, *129*, 6346.

(37) Chen, H.; Yohann, M.; Derat, E.; Shaik, S. *J. Am. Chem. Soc* **2008**, *130*, 1953.

(38) Alfonso-Prieto, M.; Borovik, A.; Carpena, X.; Murshudov, G.; Melik-Adamyan, W.; Fita, I.; Rovira, C.; Loewen, P. C. *J. Am. Chem. Soc.* **2007**, *129*, 4193.

(39) ChemShell 2.05b4 Sherwood, P.; et al. *J. Mol. Struct. (THEOCHEM)* **2003**, *632*, 1.

(40) Ahlrichs, R.; Bär, M.; Häser, M.; Horn, H.; Kölmel, C. *Chem. Phys. Lett.* **1989**, *162*, 165.

(41) Smith, W.; Forester, T. *J. Mol. Graph.* **1996**, *14*, 136.

(42) (a) Becke, A. D. *Phys. Rev. A* **1988**, *36*, 3098. (b) Lee, C.; Yang, W.; Parr, R. G. *Phys. Rev. B* **1988**, *37*, 785. (c) Becke, A. D. *J. Chem. Phys.* **1993**, *98*, 5648. (d) Becke, A. D. *J. Chem. Phys.* **1993**, *98*, 5648. (e) Becke, A. D. *J. Chem. Phys.* **1993**, *98*, 1372.

(43) MacKerell, A. D., Jr.; et al. *J. Phys. Chem. B* **1998**, *102*, 3586.

(44) Bakowies, D.; Thiel, W. *J. Phys. Chem.* **1996**, *100*, 10580.

(45) LACVP is constructed from the LANL2DZ basis sets:(a) Hay, J. P.; Wadt, W. R. *J. Chem. Phys.* **1985**, *82*, 299. (b) Friesner, R. A.; Murphy, R. B.; Beachy, M. D.; Ringlanda, M. N.; Pollard, W. T.; Dunietz, B. D.; Cao, Y. X. *J. Phys. Chem. A* **1999**, *103*, 1913.

(46) Hehre, W. J.; Ditchfield, R.; Pople, J. A. *J. Chem. Phys.* **1972**, *56*, 2257.

(47) Wachters, A. J. H. *J. Chem. Phys.* **1970**, *52*, 1033.

(48) Kühnel, K.; Derat, E.; Terner, J.; Shaik, S.; Schlichting, I. *Proc. Natl. Acad. Sci. U.S.A.* **2007**, *104*, 99.

(49) Brooks, B. R.; Bruccoleri, R. E.; Olafson, B. D.; States, D. J.; Swaminathan, S.; Karplus, M. *J. Comput. Chem.* **1983**, *4*, 187.

(50) Sicking, W.; Korth, H. G.; Jansen, G.; deGroot, H.; Sustmann, R. *Chem. Eur. J.* **2007**, *13*, 4230.

(51) (a) Schöneboom, J. C.; Neese, F.; Thiel, W. *J. Am. Chem. Soc.* **2005**, *127*, 5840. (b) Ogliaro, F.; de Visser, S. P.; Groves, J. T.; Shaik, S. *Angew. Chem., Int. Ed.* **2001**, *40*, 2874.

(52) Schöneboom, J. C.; Thiel, W. *J. Phys. Chem. B* **2004**, *108*, 7468.

(53) (a) Loew, G. H.; Harris, D. L. *Chem. Rev.* **2000**, *100*, 407. (b) Reiher, M.; Salomon, O.; Hess, B. A. *Theor. Chem. Acc.* **2001**, *107*, 48. (c) Salomon, O.; Reiher, M.; Hess, B. A. *J. Chem. Phys.* **2002**, *117*, 4729. (d) Scherlis, D.; Estrin, D. A. *Int. J. Quantum Chem.* **2002**, *87*, 158.

(54) (a) Altun, A.; Guallar, V.; Friesner, R. A.; Shaik, S.; Thiel, W. *J. Am. Chem. Soc.* **2006**, *128*, 3924. (b) Altun, A.; Shaik, S.; Thiel, W. *J. Am. Chem. Soc.* **2007**, *129*, 8978.

(55) Watanabe, Y. *J. Biol. Inorg. Chem.* **2001**, *6*, 846.

(56) As an alternative, we also tried to use Type 1 Fe^{III}-HOOH like **^{4}FeHOOH-1** as a reactant for the O−O cleavage, but the calculation indicates that the activation energy must be larger than 40 kcal/mol and that the PES describing the O−O cleavage is totally attractive at least up to an O−O distance of 2.4 Å (see Figure S10 in the Supporting Information). The absence of the H-bond to Glu183 to control the leaving OH radical also prevents its conformation from being suitable for the subsequent PCET. Therefore, it seems that Type 1 Fe^{III}-HOOH is not likely to be involved in the direct O−O activation processes.

(57) The SOC matrix element is between the orbitals π^* and $\sigma^*_{z^2}$, which is large since both orbitals have significant d(Fe) character. See ref 58 for details.

(58) Danovich, D.; Shaik, S. *J. Am. Chem. Soc.* **1997**, *119*, 1773.

(59) It is noticeable that our QM region includes the charged residues of Glu183 and His105 near the iron center and therefore bears some polarization of the protein already. The rest of the effect must reflect the bulk polarity.

(60) It should be noticed that the evolvement here concerns mainly the movement of the shared proton between Glu183 and His105 but not that of the His105 residue.

(61) (a) Sharma, P. K.; Kevorkiants, R.; de Visser, S. P.; Kumar, D.; Shaik, S. *Angew. Chem., Int. Ed.* **2004**, *43*, 1129. (b) Kumar, D.; de Visser, S. P.; Shaik, S. *J. Am. Chem. Soc.* **2005**, *127*, 8204. (c) Derat, E.; Kumar, D.; Hirao, H.; Shaik, S. *J. Am. Chem. Soc.* **2006**, *128*, 473. (d) Bach, R. D.; Dmitrenko, O. *J. Am. Chem. Soc.* **2006**, *128*, 1474.

(62) Kim, S. H.; Perera, R.; Hager, L. P.; Dawson, J. H.; Hoffman, B. M. *J. Am. Chem. Soc.* **2006**, *128*, 5598.

(63) $\hat{H} = J\,\hat{S}_A \cdot \hat{S}_B$. J is obtained from the formula $J = 2(E_Q - E_D)/(\langle S^2\rangle_Q - \langle S^2\rangle_D)$, where Q is the quartet state, and D is the doublet state. See refs 51a and 64 for details.

(64) Yamaguchi, K.; Jensen, F.; Dorigo, A.; Houk, K. N. *Chem. Phys. Lett.* **1988**, *149*, 537.

(65) Green, M. T. *J. Am. Chem. Soc.* **1999**, *121*, 7939.

(66) (a) Yoshizawa, K.; Kamachi, T.; Shiota, Y. *J. Am. Chem. Soc.* **2001**, *123*, 9806. (b) Kamachi, T.; Yoshizawa, K. *J. Am. Chem. Soc.* **2003**, *125*, 4652.

(67) (a) Ogliaro, F.; Cohen, S.; de Visser, S. P.; Shaik, S. *J. Am. Chem. Soc.* **2000**, *122*, 12892. (b) Ogliaro, F.; Cohen, S.; Filatov, M.; Harris, N.; Shaik, S. *Angew. Chem., Int. Ed.* **2000**, *39*, 3851.

(68) Schöneboom, J. C.; Lin, H.; Reuter, N.; Thiel, W.; Cohen, S.; Ogliaro, F.; Shaik, S. *J. Am. Chem. Soc.* **2002**, *124*, 8142.

(69) Derat, E.; Cohen, S.; Shaik, S.; Altun, A.; Thiel, W. *J. Am. Chem. Soc.* **2005**, *127*, 13611.

(70) Bathelt, C. M.; Mulholland, A. J.; Harvey, J. N. *J. Chem. Soc., Dalton Trans.* **2005**, *21*, 3470.

(71) Vidossich, P.; Alfonso-Prieto, M.; Carpena, X.; Loewen, P. C.; Fita, I.; Rovira, C. *J. Am. Chem. Soc.* **2007**, *129*, 13436.

JP803010F